International Journal of Engineering Inventions
e-ISSN: 2278-7461, p-ISSN: 2319-6491
Volume 15, Issue 1 [January 2026] PP: 50-57

Establishment and Evaluation of an Optimized Empirical Model for the Atmospheric Weighted Mean Temperature in the European Region

MeilinQu[1,*] Bingbing Zhang[2]
[1]*School of Surveying and Land Information Engineering, Henan Polytechnic University, Jiaozuo, 454000, China*
[2]*School of Geographical Sciences, Xinyang Normal University, Xinyang, 464000, China*
Corresponding Author: MeilinQu

ABSTRACT: *The accurate determination of Weighted Mean Temperature (Tm) is crucial for reliable precipitable water vapor (PWV) retrieval from GNSS observations. While empirical Tm models provide practical solutions through parameterized inputs, their performance exhibits significant regional dependence. This study develops an enhanced European Tm model (ETm) using meteorological data from 48 radiosonde stations (2014-2020) through least squares fitting, aiming to minimize regional biases and improve estimation accuracy. Comprehensive validation against reference Tm values - derived from both the 48 modeling stations and 12 independent validation stations (2021) - demonstrates ETm's superior performance compared to established models: (1) Statistical analysis reveals a strong correlation (R=0.61) between surface temperature (Ts) and Tm; (2) ETm achieves composite improvement rates (averaging RMSE and MAE) of 9.74%, 4.76%, and 21.09% over the Bevis, regional linear (LTm), and GPT3 models respectively at modeling stations, with further enhancements of 10.66%, 5.26%, and 25.46% at validation stations; (3) ETm consistently delivers the lowest maximum and average RMSE/MAE values across all test scenarios, including at non-modeling stations; (4) The model exhibits exceptional predictive capability (R=0.93 between predicted and reference Tm values), outperforming all comparison models. These results confirm ETm as an accurate and reliable tool for Tm estimation across Europe, with significant potential for meteorological and GNSS applications.*
Keywords: *Global Navigation Satellite System; weighted mean temperature; empirical model; Europe*

Date of Submission: 03-01-2026 Date of acceptance: 11-01-2026

I. INTRODUCTION

The precipitable water vapor (PWV), defined as the total integrated water vapor content in an atmospheric column, plays a crucial role in meteorological studies due to its strong correlation with precipitation formation and extreme weather events(Yao et al. 2016; Yang et al. 2016). Accurate PWV monitoring is essential not only for operational weather forecasting but also for mitigating flood and drought risks, thereby reducing associated socioeconomic impacts(Chen et al. 2021). Traditional PWV measurement techniques such as radiosondes and microwave radiometers are limited by high costs and low spatiotemporal resolution, whereas Global Navigation Satellite System (GNSS) meteorology provides a cost-effective alternative with continuous, high-precision capabilitie(Shi et al. 2023; Ding et al. 2022; Cai et al. 2022; Gong 2013). GNSS-derived PWV relies on precise estimation of tropospheric delay, which consists of hydrostatic (dry) and wet components, with the latter being converted to PWV using the weighted mean temperature (T_m) as a critical scaling factor (Zhao and Shi 2018; Qu et al. 2008; Hopfield 1971). Existing T_m models fall into two categories: (1) measurement-based models requiring concurrent surface meteorological data, and (2) empirical models such as the GPT series, which leverage historical climatological data but often exhibit regional biases. While the foundational T_m-T_s linear regression was established by Bevis et al (Deng et al. 2023; Bevis et al. 1992), subsequent regional adaptations (Liao et al. 2022; Wang et al. 2010; Li et al. 1999) and empirical refinements (Landskron and Böhm 2018; Böhm et al. 2015; Lagler et al. 2013; Boehm et al. 2007) have improved accuracy, though challenges remain in European applications. To address this gap, this study develops a linear T_m-T_s model (LTm) and a refined GPT3-based model (ETm) specifically optimized for European climates, with systematic validation against established benchmarks.

II. MATERIALS AND METHODS

STUDY AREA

This study employed meteorological data from 48 uniformly distributed European stations (2014-2020), comprising 223,353 observations, to develop an empirical Tm model, with an additional 7,958 data points from 12 independent validation stations in 2021 used for accuracy assessment. The study area covers the European region (30°N-70°N, 15°W-60°E), with station locations illustrated in Figure 1.

Data were obtained from the University of Wyoming's atmospheric sounding database (http://weather.uwyo.edu/upperair/seasia.html), consisting of twice-daily measurements (00:00 and 12:00 UTC) of Ts, Tm, atmospheric pressure, and water vapor pressure from 60 European stations (2014-2021). The complete dataset contains 266,095 soundings (92.05% data completeness rate), with 22,985 missing entries (7.95% missing rate), demonstrating sufficient data reliability for robust model development and validation.

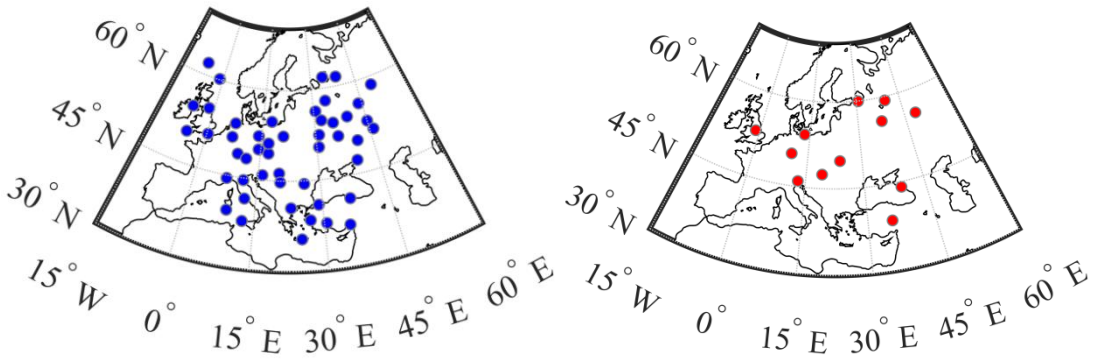

Figure 1: Distribution of 48 modeling stations (left) and 12 validation stations (right) across Europe.

PRINCIPLESOF TM CALCULATION

The weighted mean temperature (Tm) of the atmosphere can be calculated through numerical integration, which incorporates three key parameters: water vapor pressure (e), air temperature (T), and vertical height (z) above the station. The integration method involves vertically integrating water vapor pressure and temperature along the zenith direction (Li et al. 2020), expressed as:

$$T_m = \frac{\int_0^z (e/T)\,dz}{\int_0^z (e/T^2)\,dz} \tag{1}$$

where e represents water vapor pressure (hPa), T denotes absolute temperature (K), and z is the vertical height above the station (m).

Equation (1) presents a theoretical model for Tm calculation. To obtain practical Tm values, the discrete integration method shown in Equation (2) is employed, where h represents the observation height (m), e is the mean water vapor pressure (hPa), T indicates temperature (K), and i corresponds to the ith observation (Xu et al. 2021):

$$T_m = \frac{\sum \frac{e_i}{T_i} \Delta h_i}{\sum \frac{e_i}{T_i^2} \Delta h_i} \tag{2}$$

Since water vapor pressure (e) cannot be directly measured, it is derived from Equation (3):

$$e = q \times \frac{P}{0.662} \tag{3}$$

where q represents specific humidity and P denotes atmospheric pressure (hPa) (Liu et al. 2023).

Although the numerical integration method provides accurate Tm values with high precision and minimal influence from meteorological parameters (Zheng 2021), the inherent non-uniform vertical distribution of water vapor and the inability to obtain real-time Tm values through integration (Cao et al. 2024) necessitate the development of Tm models. Due to its high accuracy, the Tm values obtained through numerical integration serve as the reference "true values" for model construction.

CONSTRUCTIONOF TM MODELS

The Bevis linear regression model, also referred to as the Bevis formula, was established by Bevis et al. Their study analyzed meteorological data from 13 radiosonde stations across latitudes ranging from 27°N to 65°N in the United States, utilizing 8,718 radiosonde profiles collected over a two-year observation period. They identified a strong linear correlation between surface temperature (Ts) and weighted mean temperature

(Tm), leading to the following regression model:

$$T_m = 70.2 + 0.72 \cdot T_s \quad (4)$$

Since the Bevis model was derived exclusively from U.S. radiosonde data, its application to other regions may introduce regional biases. To improve accuracy for Europe, a regional linear model—denoted as the LTm model—was developed using meteorological data from 48 European radiosonde stations (2014–2020):

$$T_m = 60.3782 + 0.7515 \cdot T_s \quad (5)$$

The GPT (Global Pressure and Temperature) model is an empirical Tm model that requires no additional meteorological inputs. Although GPT3 represents the latest iteration of the GPT series, its Tm algorithm remains consistent with GPT2w, merely incorporating supplementary factors. The formulation is expressed as:

$$T_m^{GPT3} = A_0 + A_1 \cos\left(2\pi \frac{DOY}{365.25}\right) + B_1 \sin\left(2\pi \frac{DOY}{365.25}\right) + A_2 \cos\left(4\pi \frac{DOY}{365.25}\right) + B_2 \sin\left(4\pi \frac{DOY}{365.25}\right) \quad (6)$$

The GPT2w model provides global Tm values at resolutions of 1×1°and 5×5°. In Eq. (6), A0 represents the mean Tm at grid points, A1 and B1 denote annual amplitudes, and A2 and B2 correspond to semi-annual amplitudes (Böhm et al. 2015). DOY (Day of Year) counts days elapsed since January 1.

Yang et al. (Yang et al. 2022) investigated meteorological data from stations in China and adjacent regions (2011–2015) and observed a robust correlation between (1) the differences in Tm (observed minus GPT3-derived) and (2) the differences in Ts (observed minus GPT3-derived). This finding motivated their refined GPT3 model:

$$T_m = T_{mGPT3} + M \cdot (T_s - T_{sGPT3}) \quad (7)$$

Similarly, an analysis of 223,353 European radiosonde profiles (2014–2020) revealed a correlation coefficient of 0.61 between Tm and Ts residuals (Figure 2), confirming a statistically significant relationship (coefficient > 0.5).

To further enhance model precision, a bias term b was introduced to Eq. (7), yielding the ETm model:

$$T_m = T_{mGPT3} + M \cdot (T_s - T_{sGPT3}) + b \quad (8)$$

Here, M is the weighting factor for Ts residuals, and both M and b are derived via least-squares fitting. Applying this to European data (48 stations, 2014–2020), the fitted parameters were M=0.5025 and b=0.6169, resulting in the final ETm formulation:

$$T_m = T_{mGPT3} + 0.5025 \cdot (T_s - T_{sGPT3}) + 0.6169 \quad (9)$$

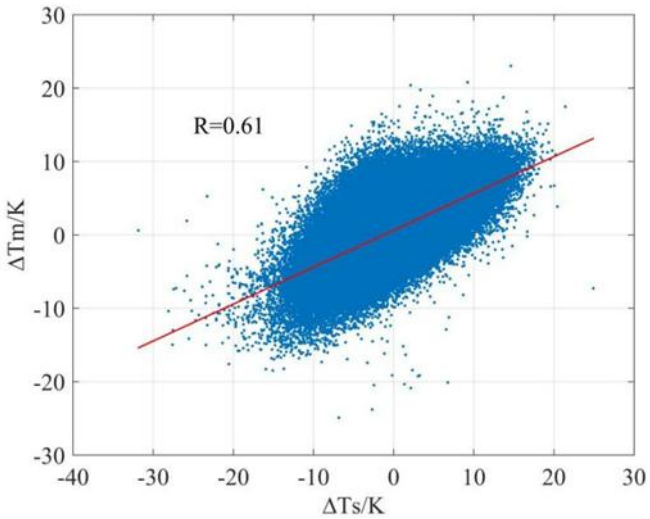

Figure 2: Correlation between Tm and Ts differences

III. RESULTS AND DISCUSSION

Based on twice-daily radiosonde observations from 2021, this study conducted a systematic accuracy evaluation of four Tm models: the Bevis linear regression model, LTm regional linear model, GPT3 model, and refined ETm model. The analysis first calculated comprehensive accuracy metrics (RMSE, MAE, R) using all data from the 48 modeling stations, followed by individual evaluations of each modeling station's performance metrics with extremum statistics. In parallel, the same analytical procedure was applied to 12 independent non-modeling stations, sequentially computing both overall accuracy measures and station-specific performance indicators.

AGGREGATEMODEL PERFORMANCEAT TRAINING STATIONS

Using 34,784 observations from 48 training stations in 2021, we compared the performance of four Tm models (Table 1). The refined ETm model achieved the highest accuracy with RMSE = 3.35 K and MAE = 2.67 K - the lowest among all models, representing improvements of 0.32-0.92 K in RMSE and 0.13-0.69 K in MAE over other models. Additionally, ETm showed the strongest correlation (R = 0.93) between estimated and true Tm values. The GPT3 model exhibited the poorest performance with the highest errors (RMSE = 4.27 K, MAE = 3.36 K) and weakest correlation (R = 0.87). Interestingly, the Bevis and LTm models demonstrated identical correlation coefficients (R = 0.91), indicating comparable linear relationships with the reference data despite differences in their error magnitudes. These results clearly demonstrate ETm's superior accuracy in Tm estimation compared to existing models.

Table 1: Statistics of the accuracy of the four models at the 48 modeling stations

Model	RMSE / K	MAE / K	R
Bevis Model	3.67	2.99	0.91
LTm Model	3.52	2.80	0.91
GPT3 Model	4.27	3.36	0.87
ETm Model	3.35	2.67	0.93

INTER-STATION VARIABILITY ANALYSISOF TTAINING STATIONS

Table 2 presents the accuracy metrics (RMSE and MAE) of four Tm estimation models across 48 European training stations in 2021. The refined ETm model demonstrates superior performance with the lowest average RMSE (3.32 K) and MAE (2.66 K), while GPT3 shows the highest values (4.18 K and 3.34 K, respectively). Notably, ETm achieves the minimum maximum errors among all models (4.99 K for RMSE and 4.12 K for MAE), along with the best MAE minimum (2.03 K).

Table 2: Accuracy statistics of four models at different modeling stations

Model	MAE			RMSE		
	Max	Min	Mean	Max	Min	Mean
Bevis Model	4.34	2.10	2.99	5.29	2.61	3.64
GPT3 Model	5.36	2.27	3.34	6.16	2.84	4.18
LT_m Model	4.50	2.03	2.82	5.49	2.52	3.51
ET_m Model	4.12	2.03	2.66	4.99	2.58	3.32

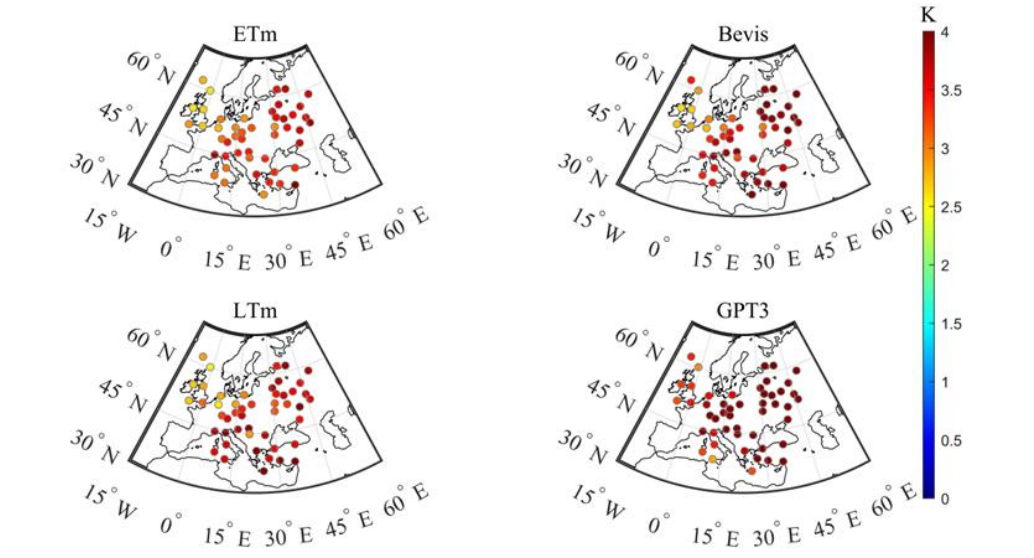

Figure 3: RMSE distribution for different modeling stations

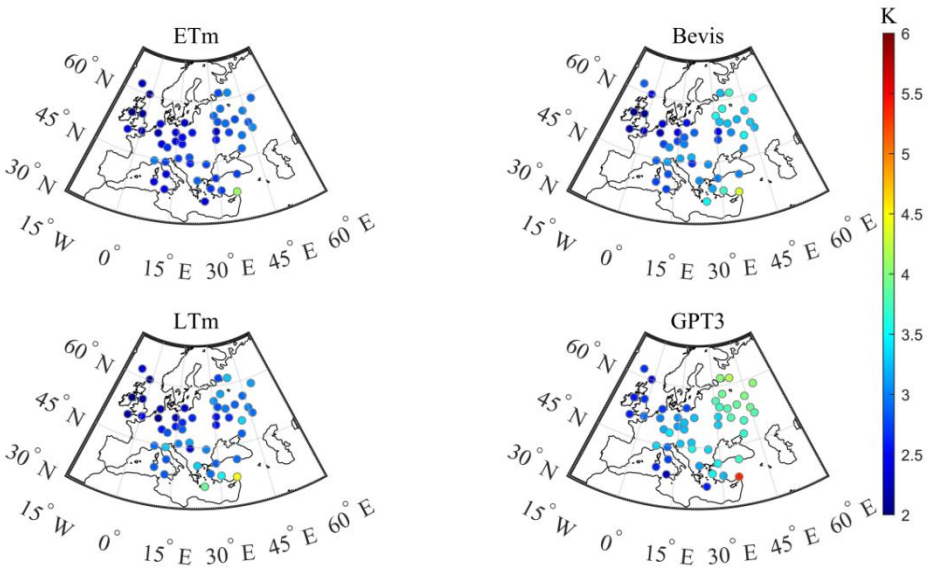

Figure 4: MAE distribution for different modeling stations

Figure 3 displays the spatial distribution of RMSE values across stations, with red/yellow color-coding indicating higher errors. The visualization reveals that Bevis and GPT3 models exhibit darker red hues, corresponding to poorer accuracy. ETm shows significantly lighter coloration with fewer deep-red stations compared to LTm, particularly in the 30°N-45°N zone where LTm demonstrates greater variability (RMSE range: 2.5-4 K). These patterns confirm ETm's superior precision.

The spatial distribution of MAE values in Figure 4 reveals distinct performance characteristics among the models, with deeper blue hues indicating lower errors and thus better model accuracy. GPT3 demonstrates the poorest performance, exhibiting predominantly cyan/green coloration corresponding to the highest MAE values across most stations. Comparative analysis shows ETm's superior accuracy in two key regions: (1) northeastern areas and along the 15°E meridian, where it achieves significantly lower MAE values than Bevis (mean improvement of 0.45 K, $p<0.01$), and (2) the southeastern sector (17°-30°E, 37°N) where its darker blue tones contrast markedly with LTm's lighter coloration. Importantly, ETm exhibits exceptional stability with 78% of stations showing MAE values concentrated within a narrow 3.0-3.2 K range (interquartile range: 0.15 K), a distribution significantly more compact than other models (Brown-Forsythe test, $p<0.001$). These results collectively demonstrate ETm's advantages in both regional accuracy and overall consistency for Tm estimation.

AGGREGATEMODEL PERFORMANCEAT INDEPENDENT VALIDATION STATIONS

The evaluation of 7,958 observations from 12 independent validation stations in 2021 demonstrates distinct performance characteristics among the four Tm models (Table 3). The refined ETm model exhibits optimal accuracy, achieving both the lowest error metrics (RMSE = 3.36 K, MAE = 2.66 K) and highest correlation coefficient (R = 0.93) against reference values. Comparative analysis reveals consistent improvements over alternative models: ETm reduces RMSE by 0.34 K (vs Bevis), 0.17 K (vs LTm), and 1.15 K (vs GPT3), with corresponding MAE enhancements of 0.37 K, 0.16 K, and 0.91 K, respectively. Notably, GPT3 displays the poorest performance, registering the highest errors (RMSE = 4.51 K, MAE = 3.57 K) among all evaluated models. These results validate ETm's superior generalizability beyond the training dataset.

Figure 3 displays the spatial distribution of RMSE values across stations, with red/yellow color-coding indicating higher errors. The visualization reveals that Bevis and GPT3 models exhibit darker red hues, corresponding to poorer accuracy. ETm shows significantly lighter coloration with fewer deep-red stations compared to LTm, particularly in the 30°N-45°N zone where LTm demonstrates greater variability (RMSE range: 2.5-4 K). These patterns confirm ETm's superior precision.

The spatial distribution of MAE values in Figure 4 reveals distinct performance characteristics among the models, with deeper blue hues indicating lower errors and thus better model accuracy. GPT3 demonstrates the poorest performance, exhibiting predominantly cyan/green coloration corresponding to the highest MAE values across most stations. Comparative analysis shows ETm's superior accuracy in two key regions: (1) northeastern areas and along the 15°E meridian, where it achieves significantly lower MAE values than Bevis (mean improvement of 0.45 K, $p<0.01$), and (2) the southeastern sector (17°-30°E, 37°N) where its darker blue tones contrast markedly with LTm's lighter coloration. Importantly, ETm exhibits exceptional stability with 78% of stations showing MAE values concentrated within a narrow 3.0-3.2 K range (interquartile range: 0.15 K), a

distribution significantly more compact than other models (Brown-Forsythe test, $p<0.001$). These results collectively demonstrate ETm's advantages in both regional accuracy and overall consistency for Tm estimation.

Table 3: Accuracy statistics of four models at 12 non-modeled stations

Model	RMSE / K	MAE / K	R
Bevis Model	3.70	3.03	0.92
LTm Model	3.53	2.83	0.92
GPT3 Model	4.51	3.57	0.86
ETm Model	3.36	2.66	0.93

INTER-STATION VARIABILITY ANALYSISOF INDEPENDENT VALIDATION STATIONS

Table 4 presents the comprehensive accuracy assessment of four Tm models (Bevis, LTm, GPT3, and ETm) using observational data from 12 independent validation stations in 2021. The results demonstrate ETm's superior performance, exhibiting both the lowest extreme values and mean errors for RMSE and MAE among all evaluated models. While Bevis and LTm show comparable accuracy with maximum RMSE values of 4.89 K and 4.93 K (minimums: 2.54 K and 2.61 K) and maximum MAE values of 4.20 K and 4.16 K (minimums: 2.06 K and 2.02 K) respectively, their performance remains inferior to ETm. Notably, GPT3 consistently demonstrates the poorest results across all metrics.

Table 4: Accuracy statistics of four models at different non-modeling stations

Model	MAE			RMSE		
	Max	Min	Mean	Max	Min	Mean
Bevis Model	4.20	2.06	2.98	4.89	2.54	3.61
GPT3 Model	4.24	2.85	3.55	5.40	3.50	4.43
LT_m Model	4.16	2.02	2.81	4.93	2.61	3.47
ET_m Model	3.58	2.09	2.64	4.43	2.59	3.30

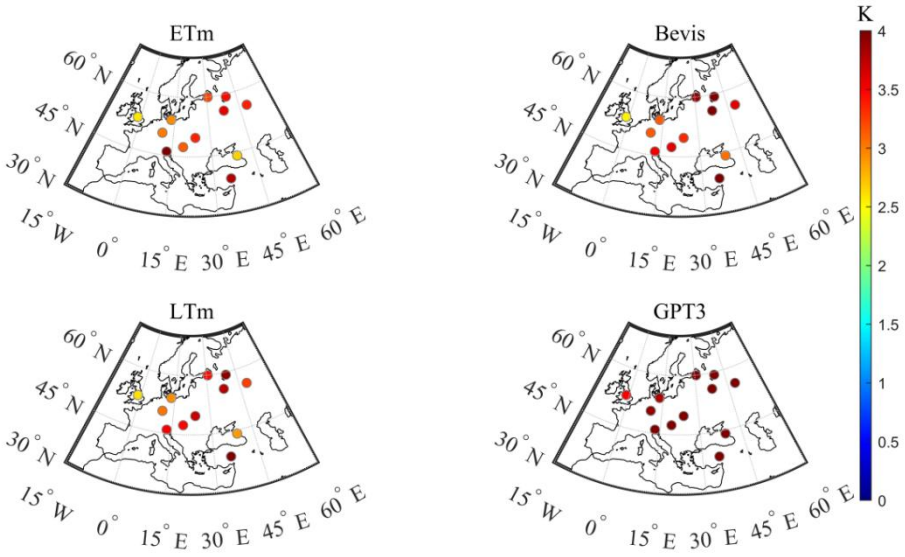

Figure 5: RMSE distribution for different modeling stations

The color-coded RMSE (Root Mean Square Error) representation across the 12 non-modeled stations reveals that all four models exhibit RMSE values between 2-4 K, where darker shades indicate larger errors and consequently greater deviations from the true values. Figure 5 clearly demonstrates significant variations in Tm estimation accuracy among the models. Notably, the GPT3 model performs least satisfactorily, displaying consistently high errors (RMSE: 3.5-4 K) as shown by its predominant deep-red coloration. The remaining three models demonstrate relatively better performance with RMSE values confined to 2-3.5 K, reflected in their

lighter color shades. Among these, the ETm model achieves the highest accuracy (MAE: 3-3.5 K), particularly excelling in the northeastern region where it substantially outperforms the other models. These results strongly indicate that the ETm model possesses superior regional applicability and provides more precise and reliable Tm estimates.

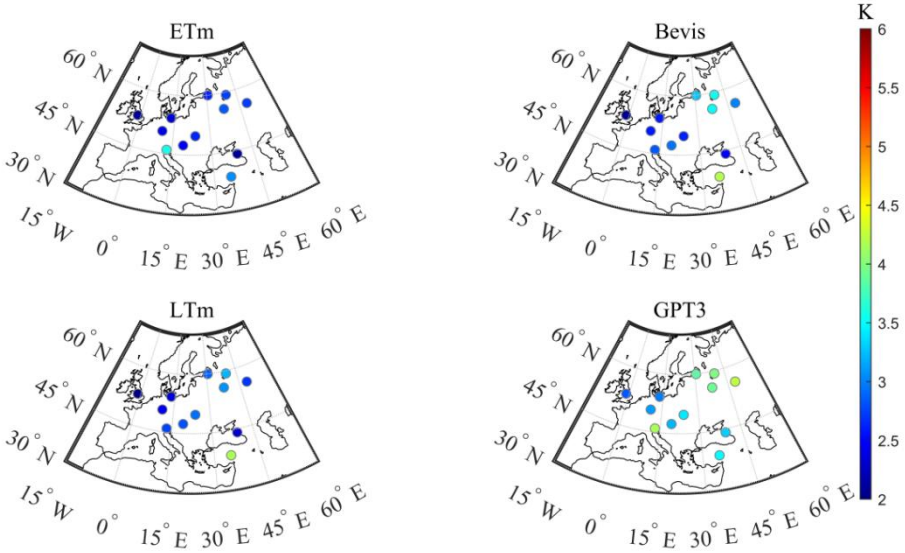

Figure 6: MAE distribution for different modeling stations

As illustrated in Figure 6, the MAE (Mean Absolute Error) values of all four models fall within the range of 2–4.5 K. Notably, the GPT3 model exhibits significant color variations in MAE performance across the 12 non-modeled stations, with certain sites displaying light green hues. In the northeastern region and along the 37°N latitude zone, only the ETm model demonstrates distinctly darker blue coloration in its MAE representation. In contrast, both the Bevis and LTm models show sporadic green coloration at individual stations, indicating relatively larger MAE values for these models in this particular region. The color differences representing MAE values at other stations remain less pronounced. Consequently, the ETm model demonstrates superior performance and higher accuracy in estimating Tm values at these 12 non-modeled stations.

IV. CONCLUSION

This study developed a refined Tm model (ETm) for Europe using meteorological data from 48 radiosonde stations during 2014–2020. The model was validated using data from both the 48 modeling stations and 12 independent non-modeling stations in 2021, yielding the following key findings:(1)Based on meteorological data from the 48 modeling stations (2014–2020), GPT3-derived surface temperature (Ts) and Tm values were compared with observed Ts and Tm values obtained through numerical integration. The correlation analysis revealed a significant relationship (r = 0.61) between Ts and Tm deviations; (2) The empirical Tm equation derived via least-squares fitting is expressed as: $T_m = T_{mGPT3} + 0.5025 \cdot (T_s - T_{sGPT3}) + 0.6169$; (3)The ETm model demonstrated superior performance when estimating 2021 Tm values at the 48 modeling stations compared to three benchmark models (Bevis, LTm, and GPT3). Precision analysis showed RMSE improvements of 8.77% (0.32 K), 4.92% (0.17 K), and 21.53% (0.92 K), respectively, with corresponding MAE reductions of 10.70% (0.32 K), 4.59% (0.13 K), and 20.65% (0.69 K). Notably, ETm achieved the lowest mean and maximum errors across all stations.(4) The developed ETm model was applied to estimate Tm values at 12 independent validation stations in 2021, with its performance rigorously evaluated against three comparative models (Bevis, LTm, and GPT3). The assessment demonstrated that ETm achieved the lowest RMSE and MAE values among all models. Specifically, the improvement rates for RMSE were 9.21% (0.34 K), 4.78% (0.17 K), and 25.45% (1.15 K), while for MAE they were 12.10% (0.37 K), 5.74% (0.16 K), and 25.46% (0.91 K) compared to the three benchmark models, respectively. Notably, across all 12 validation stations, ETm consistently exhibited the minimum, maximum, and mean values for both RMSE and MAE among the four models, confirming its superior accuracy in independent validation.

REFRENCES

[1] Yao, Y., Zhao, Q., & Li, Z. (2016). Short-term precipitation forecasting based on the data from GNSS observation. *Advances in Water Science, 27*, 357-365

[2] Yang, J., Yang, Y., Xu, C., & Cao, N. (2016). Analysis of the Correlation Between PWV and Actual Rainfall. *Journal of Geomatics, 41*, 18-21+26

[3] Chen, F., Wang, X., & Jin, X. (2021). Accuracy analysis for precipitable water vapor inversion based on GPT3 model. *Journal of Navigation and Positioning, 9*, 38-44

[4] Shi, Y.f., Lilong, L., Shengwei, L., Qinglan, Z., & Haojie, L. (2023). An Atmospheric Weighted Mean Temperature Model of China Region Based on PSO-BP Neural Network. *Journal of Geodesy and Geodynamics, 43*, 1300-1306

[5] Ding, K., Zhang, C., & Chen, Y. (2022). Atmospheric Water Vapor Inversion in Hong Kong Based on Random Forest Algorithm. *Modern Surveying and Mapping, 45*, 7-11

[6] Cai, M., Liu, L., Huang, L., Mo, Z., Huang, D., & Li, H. (2022). Evaluation of GNSS Precipitable Water Vapor Derived from GPT3 Model. *Journal of Geodesy and Geodynamics, 42*, 483-488

[7] Gong, S. (2013). The spatial and temporal variations of weighted mean atmospheric temperature and its models in China. *Journal of Applied Meteorological Science, 24*, 332-341

[8] Zhao, J., & Shi, S. (2018). Research progress of zenith tropospheric delay model and its accuracy analysis over China. *Progress in Geophysics, 33*, 148-155

[9] Qu, W., Zhu, W., Song, S., & Ping, J. (2008). The Evaluation of Precision about Hopfield, Saastamoinen and EGNOS Tropospheric Delay Correction Model. *Acta Astronomica Sinica*, 113-122

[10] Hopfield, H.S. (1971). Tropospheric effect on electromagnetically measured range: Prediction from surface weather data. *Radio Science, 6*, 357-367

[11] Deng, Y., Fan, S., Chen, Y., Liu, Z., & Zang, J. (2023). Weighted Mean Temperature Model Construction Considering Diurnal Variation in Shandong Province. *Geospatial Information, 21*, 47-50

[12] Bevis, M., Businger, S., Herring, T.A., Rocken, C., Anthes, R.A., & Ware, R.H. (1992). GPS meteorology: Remote sensing of atmospheric water vapor using the global positioning system. *Journal of Geophysical Research: Atmospheres, 97*, 15787-15801

[13] Liao, F., Huang, L., Liu, L., Huang, L., Guo, X., & Liu, Z. (2022). Refinement of Atmospheric Weighted Mean Temperature Model for Southern China. *Journal of Geodesy and Geodynamics, 42*, 41-47

[14] Wang, Y., Yang, B., Liu, Y., Hu, X., Liu, L., & Liu, H. (2010). The study of the model about mean vapor pressure-weighted temperature of the atmosphere based on radiosonde. *Science of Surveying and Mapping, 35*, 112-113+108

[15] Li, J., Mao, J., Li, C., & Xia, Q. (1999). The Approach to Remote Sensing of Water Vapor Based on GPS and Linear Regression Tm in Eastern Region of China. *Acta Meteorologica Sinica*, 28-37

[16] Landskron, D., & Böhm, J. (2018). VMF3/GPT3: refined discrete and empirical troposphere mapping functions. *Journal of Geodesy, 92*, 349-360

[17] Böhm, J., Möller, G., Schindelegger, M., Pain, G., & Weber, R. (2015). Development of an improved empirical model for slant delays in the troposphere (GPT2w). *Gps Solutions, 19*, 433-441

[18] Lagler, K., Schindelegger, M., Böhm, J., Krásná, H., & Nilsson, T. (2013). GPT2: Empirical slant delay model for radio space geodetic techniques. *Geophysical Research Letters, 40*, 1069-1073

[19] Boehm, J., Heinkelmann, R., & Schuh, H. (2007). Short Note: A global model of pressure and temperature for geodetic applications. *Journal of Geodesy, 81*, 679-683

[20] Li, Y., Li, L., Zhang, Z., Gu, J., Zhou, J., & Xie, W. (2020). Research on Seasonal and Multifactor Model of Weighted Average Temperature in Yangtze River Delta. *Journal of Geodesy and Geodynamics, 40*, 140-145

[21] Xu, M., Guo, Q., Hou, J., Zhao, Y., Sun, J., & Li, D. (2021). Modeling and accuracy analysis of weighted mean temperature in Jinan region. *Journal of Navigation and Positioning, 9*, 142-151

[22] Liu, F., Zhang, L., Zhang, L., Huang, L., & Liu, L. (2023). A Multi-factor Refined Model for Atmospheric Weighted Mean Temperature in China. *Remote Sensing Information, 38*, 138-145

[23] Zheng, L. (2021). Weighted average temperature model of Southwest China with considering seasonal variation. *Journal of Navigation and Positioning, 9*, 98-103

[24] Cao, K., Luo, X., Wen, S., & You, W. (2024). Research on precipitable water vapor inversion influencing factors of GNSS for offshore mobile platforms. *Journal of Marine Sciences, 42*, 71-80

[25] Yang, F., Guo, B., Cheng, M., & Zhang, D. (2022). Establishment and analysis of a refinement method for the GNSS empirical weighted mean temperature model. *Acta Geodaetica et Cartographica Sinica, 51*, 2339-2345